ADVANCED MATERIALS

Supporting Information

for *Adv. Mater.*, DOI: 10.1002/adma.201304949

Large Arrays and Properties of 3-Terminal Graphene Nanoelectromechanical Switches

*Xinghui Liu, Ji Won Suk, Narasimha G. Boddeti, Lauren Cantley, Luda Wang, Jason M. Gray, Harris J. Hall, Victor M. Bright, Charles T. Rogers, Martin L. Dunn, Rodney S. Ruoff, and J. Scott Bunch**

Submitted to ADVANCED MATERIALS

DOI: 10.1002/adma.201304949

Supporting Information: Large Arrays and Properties of 3-Terminal Graphene Nanoelectromechanical Switches

By *Xinghui Liu*, *Ji Won Suk*, *Narasimha G. Boddeti*, *Lauren Cantley*, *Luda Wang*, *Jason M. Gray*, *Harris J. Hall*, *Victor M. Bright*, *Charles T. Rogers*, *Martin L. Dunn*, *Rodney S. Ruoff*, and *J. Scott Bunch* *

[*] Prof. J. Scott Bunch, Xinghui Liu, Narasimha G. Boddeti, Lauren Cantley, Luda Wang, Dr. Jason M. Gray, Dr. Harris J. Hall, Prof. Victor M. Bright
Department of Mechanical Engineering
University of Colorado, Boulder, CO 80309 USA
Prof. J. Scott Bunch (current address)
Department of Mechanical Engineering and Division of Materials Science and Engineering
Boston University, Boston, MA 02215 USA
E-mail: (bunch@bu.edu)
Dr. Ji Won Suk, Prof. Rodney S. Ruoff
Department of Mechanical Engineering and the Materials Science and Engineering Program, The University of Texas, Austin, TX 78712 USA
Prof. Charles T. Rogers
Department of Physics
University of Colorado, Boulder, CO 80309 USA
Prof. Martin L. Dunn
Singapore University of Technology and Design,
Singapore, 138682

Keywords: Graphene, Nanoelectromechanical Systems, Microsystems, Nanomechanical Switches, Finite Element Analysis

Supporting Information:

S.1 Device Fabrication

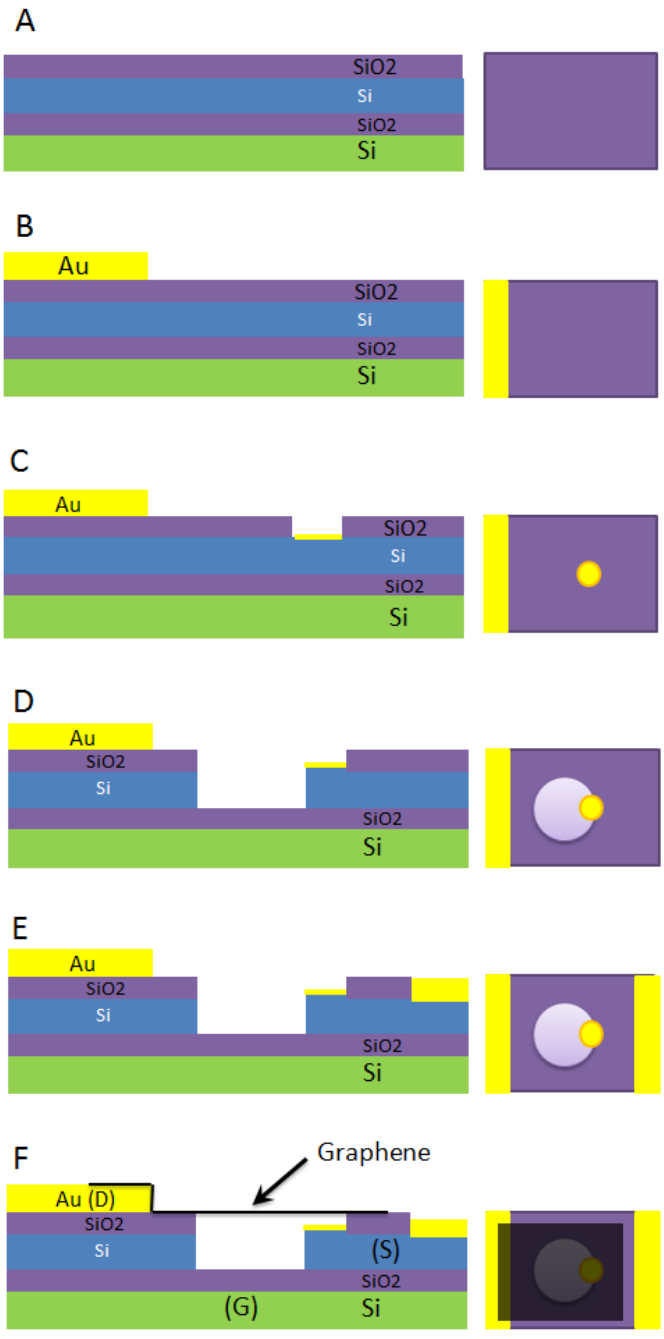

Figure S1. Schematic of process flow for fabrication of CVD graphene 3-terminal switches

The predefined wells over which graphene is transferred are fabricated by a combination of standard micro-fabrication processes on SOI wafers (device silicon layer 1μm thick, buried oxide layer 100/200 nm thick, handle silicon layer 500μm thick). At first, the device layer is etched by reactive ion etching (RIE) with SF_6 down to 270-300 nm, and then the device layer is heavily doped by boron diffusion. Thermal oxidation is used to grow a layer of 150-200 nm thick SiO_x on the device Si layer of an SOI wafer (Fig. S1A). An array of 220 μm x 220 μm Au electrodes (drain electrodes) are patterned using photolithography followed by thermal evaporation of 5/50 nm of Cr/Au (Fig. S1B). The wells, over which graphene membranes are suspended, are etched next to the drain electrodes. First, an array of ~ 2 μm circular wells are etched through the top SiO_x layer by reactive ion etching (RIE), and a layer of 5/30 nm Cr/Au is thermally evaporated into the wells to define the source electrodes (Fig. S1C). Then, larger circular wells (~5 μm diameter) are etched overlapping each source electrode and through both the SiO_x layer and the Si device layer with a combination of buffered oxide etching (BOE 1:6) and RIE (Fig. S1D-E). Finally, each chip is separated into arrays of units by trenches (15 μm wide) etched down to the buried oxide layer, and each unit is prepared for four potential devices. In each unit, two windows (200 μm x 80 μm) to the underneath source electrode are fabricated by RIE etching the top oxide layer and depositing a layer of Cr/Au (5/60 nm).

Graphene sheets are prepared by chemical vapor deposition (CVD) on copper foil, and then patterned with oxygen plasma into arrays of 50 μm x 12 μm rectangular strips.[1] Graphene sheets were transferred onto the substrates using a dry transfer method.[2] (Fig. S1F)

S.2 Finite Element Modeling

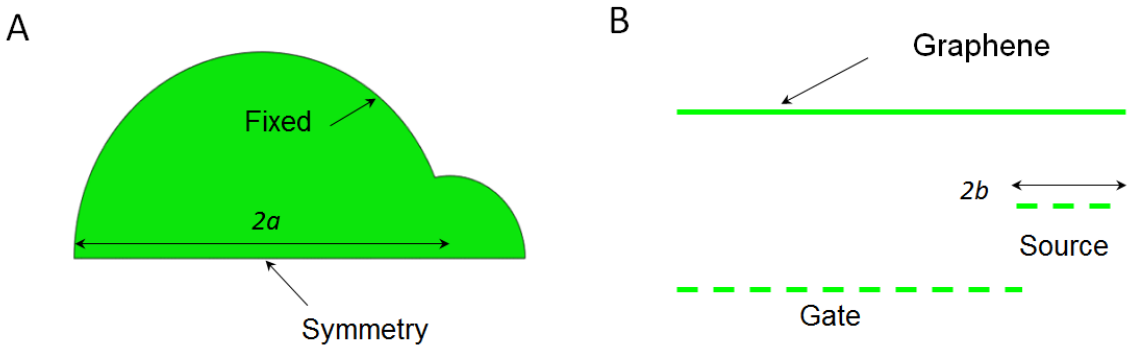

Figure S2. Models for finite element analysis. (A) Top view of a simplified finite element model (Abaqus) of graphene membrane in the NEMS switch. **(B)** Side view of the finite element model. $2a$ = 5 µm, $2b$ = 2 µm, d_1 = 120 nm, d_2 = 230 nm, and d_3 = 200 nm.

The schematic of the switch is as shown in Fig. S2A. The switch can operate either in 2-terminal or 3-terminal configurations, the difference being that in the 2-terminal operation V_g is set to zero. The simplified finite element (FE) model is also shown in Fig. S2B. The suspended graphene membrane (drain) is the deformable electrode while the source and gate are rigid and fixed. Hence only the deformable part of the graphene membrane is actually part of the FE model while the rest of the switch is modeled through constraints and loads. The graphene membrane is fixed along the edges and advantage is taken of the two fold symmetry by applying a symmetry boundary condition. The electrostatic forces due to the electric fields between the drain and source electrodes as well as the drain and gate electrodes that deform the graphene membrane are described by equations (1) and (2) in the main text. These position dependent loads have been applied using DLOAD sub-routine of Abaqus.[3] The graphene membrane is

modeled with S4R (4 noded shell elements with reduced integration) elements to include both bending and stretching effects.[4, 5]

As the electrostatic load is increased, the membrane deforms and comes closer to the electrodes and at the threshold voltage, pulls-in, thereby making contact and completing the circuit. This contact occurs along the axis of symmetry at the edge of the post (source electrode). We call the deflection of the membrane at this point the "edge deflection". In the two-terminal operation, the pull-in is caused solely by V_{sd} while in the three-terminal operation it is caused by increasing V_g. The results show that the pull-in in the three-terminal case is a local phenomenon as the maximum deflection that occurs near the center of the suspended region along the axis of symmetry shows no abrupt change with increasing V_g.

S.3 Additional Experimental Results to Verify the Electromechanical Switching

To rule out purely electrical effects in the switching behavior, we did some additional experiments to distinguish the IV characteristics from graphene NEMS switches and graphene-Si Schottky barriers, and then to verify that the measured electrical IV characteristics come from the electromechanical actuated movements.

The electrostatic force that deflects the graphene membrane, $F_e = - V^2 A\varepsilon_0\varepsilon_r / 2d^2$, is symmetric with respect to the sign, where V is the applied voltage, A is the area of the membrane, ε_0 is the dielectric permittivity of vacuum space, ε_r is the dielectric constant, and d is the distance between the graphene membrane and the underneath electrode. Therefore, switching should be symmetric for positive and negative voltages, which is indeed the case. One example is shown in Fig. S3. For two-terminal switching with positive and negative V_{sd}, the threshold V_{sd} is ~ 6 V and ~ -6 V respectively (Fig. S3A).

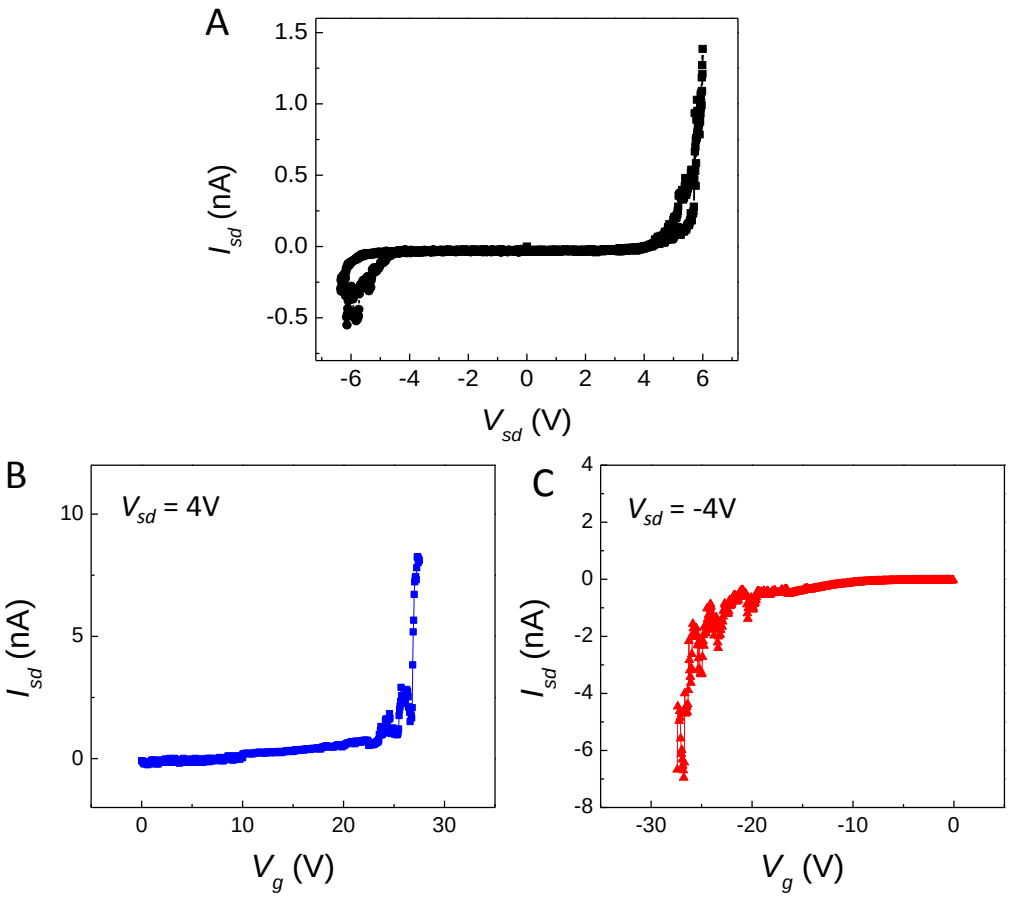

Figure S3. Switching in positive and negative actuation voltages. (A) 2-terminal IV characteristic with positive and negative V_{sd}. (B) 3-terminal IV characteristic with positive V_{sd} and V_g. (C) 3-terminal IV characteristic with negative V_{sd} and V_g.

Three terminal switching from the same device demonstrates similar symmetry. When sweeping the gate voltage in the positive range with V_{sd} = 4 V, the threshold V_g is ~ 28V (Fig. S3B). For the opposite case, the threshold V_g is ~ -28 V with V_{sd} = -4 V (Fig. S3C). However, this kind of symmetry is not observed in graphene-Si Schottky barriers.[6, 7]

In addition, we checked if the graphene membrane in the device from which we took the data in Fig. S3 is suspended with atomic force microscope (AFM) imaging before and after these electrical measurements to rule out the possibility that the

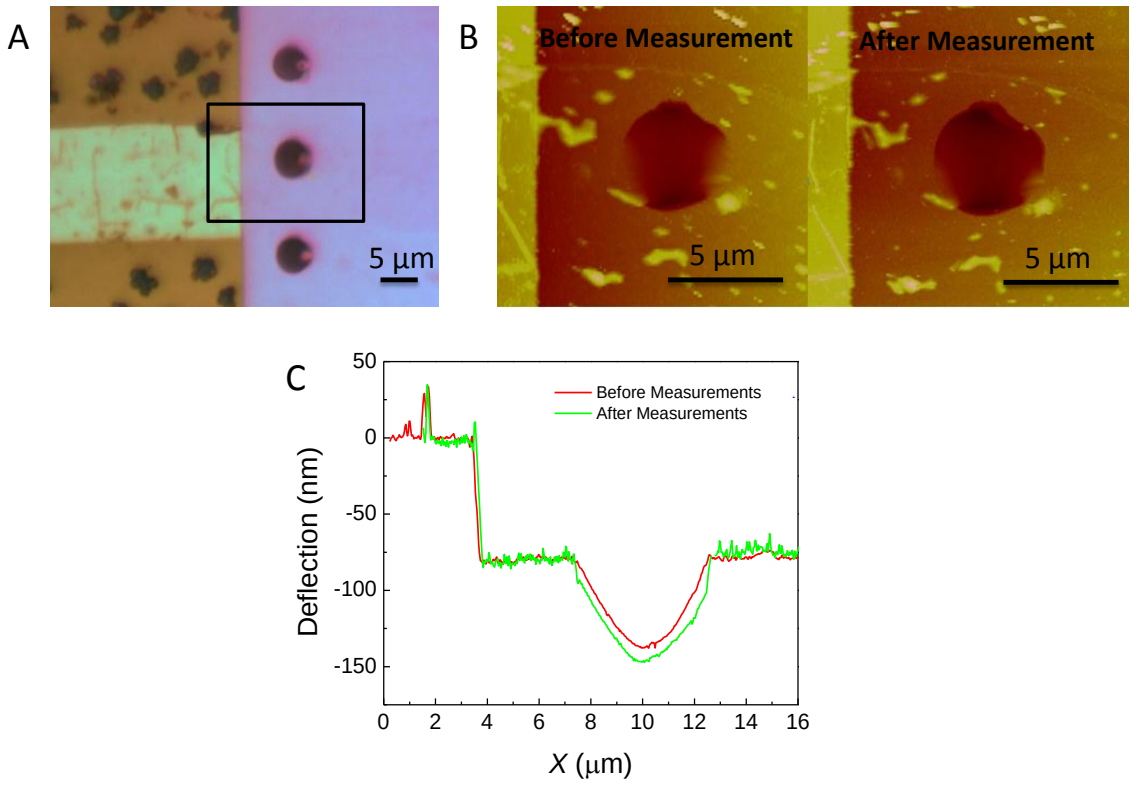

Figure S4. (A) Optical image of the graphene NEMS switch we took the data in Fig. S3. (B) AFM images of the graphene membrane in the device (in the black rectangle) before and after the electrical measurements shown in Fig. S3. (C) Cross cuts of the AFM images before and after electrical measurements across the center of the graphene membrane.

graphene membrane got stuck to the electrodes before measurement. The AFM images of the suspended graphene membrane in the device before and after the electrical measurements are shown in Fig. S4B, and the images are of the same color scale. We observed that the graphene membrane remained free standing before and after the electrical measurement as shown in Fig. S3. From the crosscuts of the AFM images in Fig. S4C, we also found that the graphene membrane dipped in about 10 nm, most likely

due to slack introduced in the graphene from transfer process. This phenomenon can be considered as further evidence of the electromechanical switching in the device.

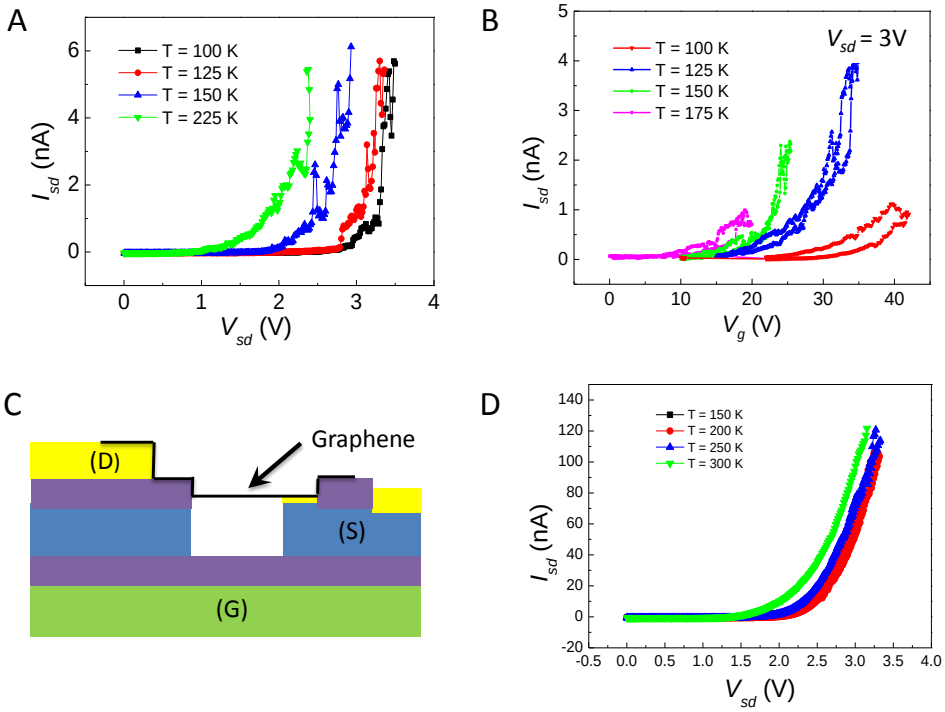

Figure S5. Temperature dependence measurement. (A) Two-terminal switching at different temperatures from 100 K to 225K. (B) Three-terminal switching at different temperatures from 100 K to 175 K. (C) Schematic of a switch with graphene stuck to the source electrode. (D) IV_{sd} characteristic of the "stuck device".

We also studied the temperature dependence of the threshold switching voltages in the graphene NEMS switches and compared it with that of "stuck" devices. Fig. S5A shows the 2-terminal switching IV curves at four different temperatures ranging from 100 K to 225 K. With the increase of temperature, the threshold V_{sd} voltage decreases. The three terminal switching shows a similar dependence (Fig. S5B). With the temperature increase from 100 K to 175 K, the switching V_g decrease from more than 42 V to ~18 V

with V_{sd} = 3V. The apparent temperature dependence can be attributed to an increase in the tension on suspended graphene with decrease of temperature, which has been observed for both CVD and exfoliated suspended graphene membranes.[8, 9] In comparison, the IV_{sd} traces for this device after being "stuck", the schematic of which is shown in Fig. S5C, for temperatures from 150 K to 300 K showed very limited temperature dependence in contrast to the data in Fig. S5D.

S4. Graphene 3-Terminal Switches with a Different Geometry

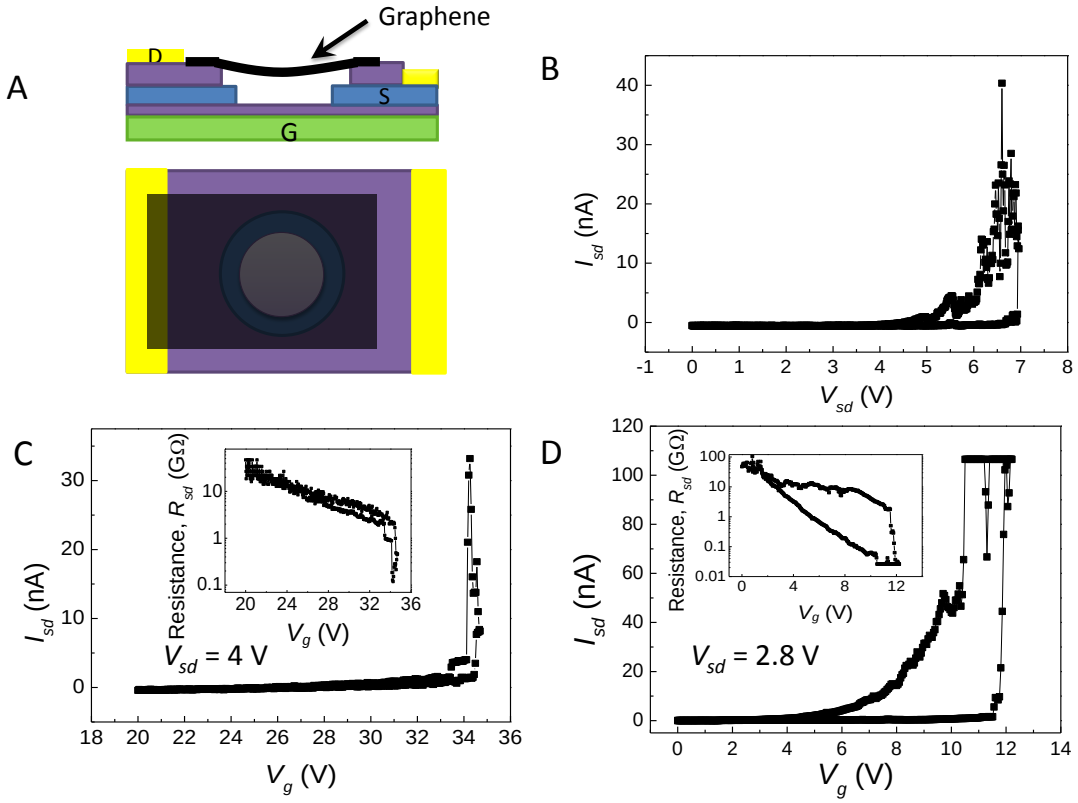

Figure S6 Experimental data of a graphene NEMS switch with a different geometry. (A) (upper) Side-view schematic of the switch. (lower) Top-view of the switch. (B) Two-terminal IV characteristic of a graphene NEMS switch with the geometry in Fig. S6A. (C) Three-terminal IV characteristic of the switch at 78 K and a pressure of ~10^{-6} Torr. (D) Three-terminal IV characteristic of a switch with geometry in Fig. S6A at room temperature and atmosphere.

We developed a different geometry for the graphene NEMS switches. The side view schematic and top view of the switch is shown in Fig. S6A. Instead of a Au coated circular source electrode at the edge of the predefined well on which graphene membrane is suspended, a uniform step around the edge of the well is etched with BOE 1:6 and the exposed heavily doped device Si layer is exposed as the source electrode. The width of the step is 0.3 – 1 μm, and the depth of the step (d_1) above the source electrodes ranges from 100 nm to 220 nm as well. An example of switching IV characteristics of a

graphene NEMS switch is shown in Figure S6B and S6C. The threshold V_{sd} and V_g are 7 V and 34.5 V, respectively. Figure S6D shows a switching IV curve for a three-terminal switch at room temperature. The threshold V_g is ~12V with V_{sd} = 2.8 V, close to the requirement for CMOS IC integration.[10]

S5. More AFM measurement results before and after electrical measurements

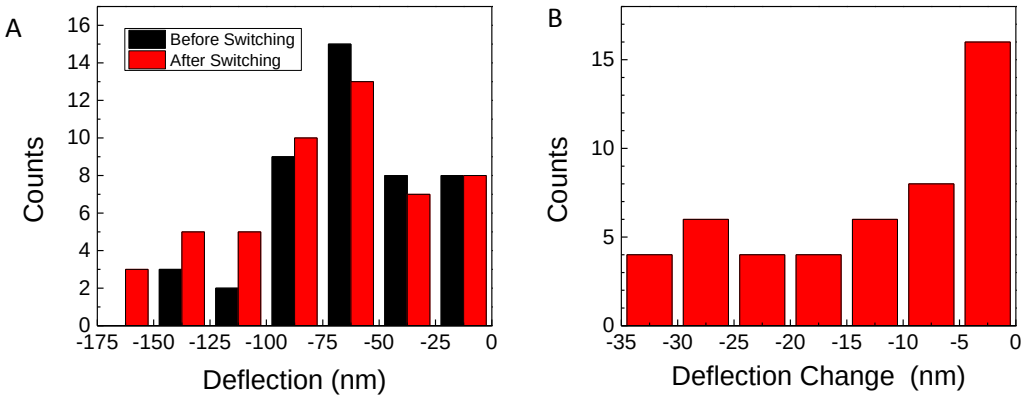

Figure S7 (A) Statistical distribution of center deflections measured by AFM of graphene membranes from one chip before and after ~10 times electrical switching. (B) Statistical distribution of the change of center deflection after the electrical measurements.

We took AFM images before and after the electrical measurements of more than 100 suspended graphene membrane devices. The statistical distribution of the center deflections of the graphene membranes from 49 devices on one chip before and after 1-10 times of electromechanical switching is shown in Fig. S7A. The majority of the center deflections before and after electrical measurements are 50-100 nm downward, while the depth of the underneath source electrodes is ~200 nm. After electromechanical switching, most of the graphene membranes have a larger initial deflection, and the deflection changes are plotted in Fig. S7B. These changes range from 0 nm to 35 nm with the majority being within 10 nm.

Fig. S8 shows one example of the comparison between AFM images from devices with suspended and stuck graphene membranes after the electrical measurements. For device I in Fig. S8A, the graphene membrane stayed suspended after the measurements (in Fig. S8C and Fig. S8D), and the membrane remained free standing even though the initial deflection changed some, presumably due to slack introduced during the mechanical switching (Fig. S8B). For device II in Fig. S8E, the graphene membrane got stuck onto the underneath source electrode as seen in the AFM image.

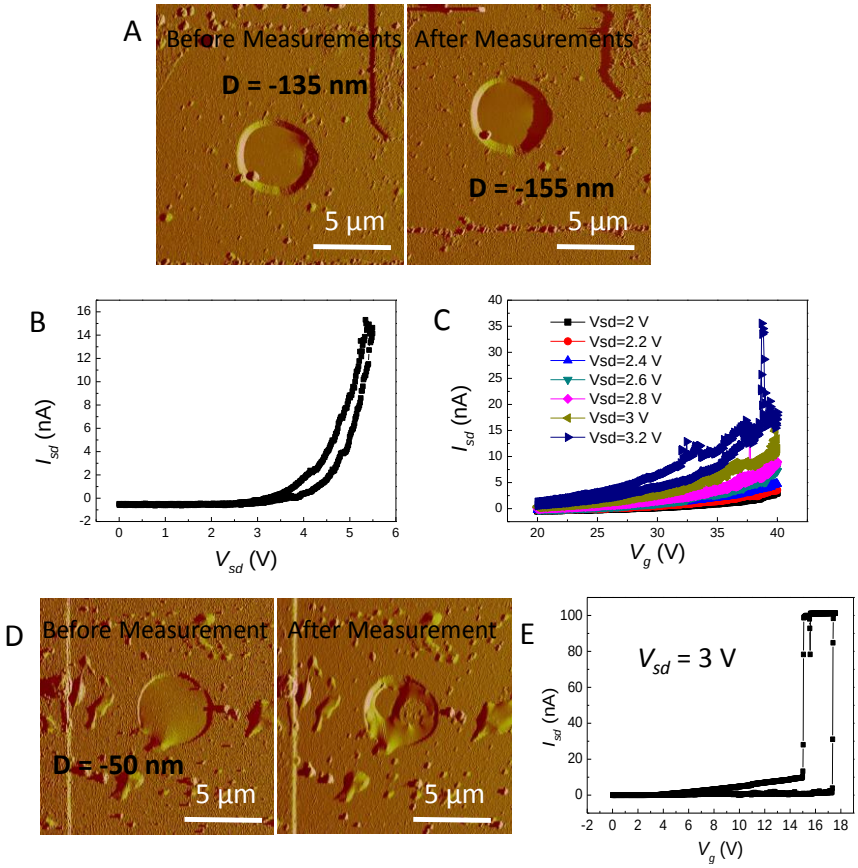

Figure S8. Additional AFM images before and after the electrical measurement. (A) AFM Amplitude images of the graphene membrane in device I before and after the electrical measurements. Before the electrical measurements, the center deflection of the membrane is -135 nm, and after is -155 nm. (B) A *IV* curve showing a 2-terminal switch in device I. (C) *IV* curves of 3-terminal switching with V_{sd} changing from 2 V to 3.2 V with an increment of 0.2 V in device I. (D) AFM Amplitude images of the graphene membrane in device II before and after the electrical measurements. Before the electrical measurements, the center deflection of the membrane is -50 nm, and after the switching, the membrane got stuck to the bottom of the microcavity and had a deflection of -190 nm at the electrode part and -300 nm at the bottom of the microcavity. (E) *IV* curves of 3-terminal switching in device II with V_{sd} =3 V, during which graphene got stuck.

References

[1]. Li, X.; Cai, W.; An, J.; Kim, S.; Nah, J.; Yang, D.; Piner, R.; Velamakanni, A.; Jung, I.; Tutuc, E.; Banerjee, S. K.; Colombo, L.; Ruoff, R. S. *Science* **2009,** 324, (5932), 1312-1314.

[2]. Suk, J. W.; Kitt, A.; Magnuson, C. W.; Hao, Y.; Ahmed, S.; An, J.; Swan, A. K.; Goldberg, B. B.; Ruoff, R. S. *ACS Nano* **2011,** 5, (9), 6916-6924.

[3]. Hibbitt, K., Sorensen, *ABAQUS/Standard: user's manual*. Dassault Systèmes Simulia Corp.: Providence, RI, USA, 2011.

[4]. Shenoy, V. B.; Reddy, C. D.; Zhang, Y.-W. *ACS Nano* **2010,** 4, (8), 4840-4844.

[5]. Pantano, A.; M. Parks, D.; Boyce, M. C. *Journal of the Mechanics and Physics of Solids* **2004,** 52, (4), 789-821.

[6]. Yang, H.; Heo, J.; Park, S.; Song, H. J.; Seo, D. H.; Byun, K.-E.; Kim, P.; Yoo, I.; Chung, H.-J.; Kim, K. *Science* **2012,** 336, (6085), 1140-1143.

[7]. Chen, C.-C.; Aykol, M.; Chang, C.-C.; Levi, A. F. J.; Cronin, S. B. *Nano Letters* **2011,** 11, (5), 1863-1867.

[8]. Zande, A. M. v. d.; Barton, R. A.; Alden, J. S.; Ruiz-Vargas, C. S.; Whitney, W. S.; Pham, P. H. Q.; Park, J.; Parpia, J. M.; Craighead, H. G.; McEuen, P. L. *Nano Letters* **2010,** 10, (12), 4869-4873.

[9]. Chen, C.; Rosenblatt, S.; Bolotin, K. I.; Kalb, W.; Kim, P.; Kymissis, I.; Stormer, H. L.; Heinz, T. F.; Hone, J. *Nat Nano* **2009,** 4, (12), 861-867.

[10]. Czaplewski, D. A; Patrizi, G. A; Kraus, Garth M.; Wendt, J. R.; Nordquist, C. D.; Wolfley, S. L.; Baker, M. S.; de Boer, M. P. *Journal of Micromechanics and Microengineering* **2009,** 19, (8), 085003.